PAPER • **OPEN ACCESS**

Preparation of multilayer samples for scanning thermal microscopy examination

To cite this article: James Lees *et al* 2024 *Nanotechnology* **35** 225702

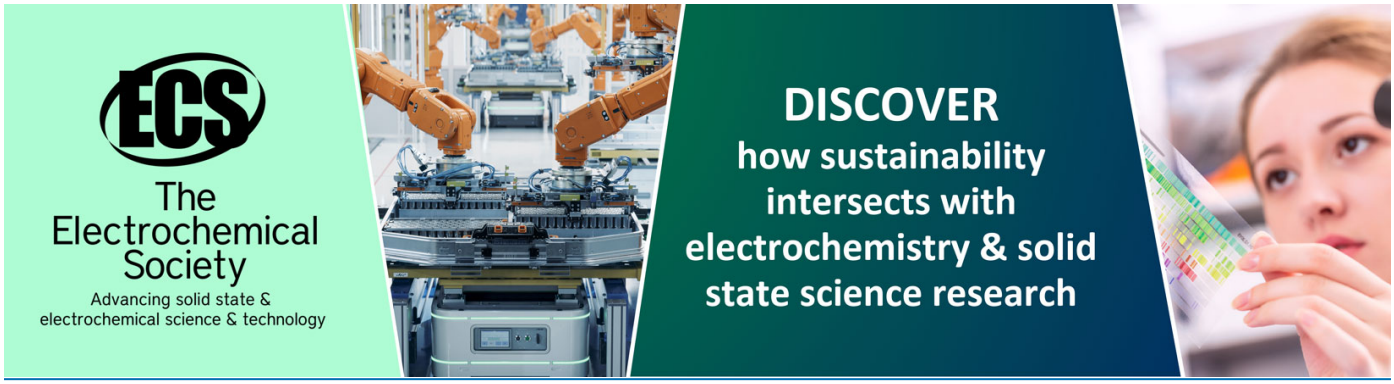

OPEN ACCESS
IOP Publishing
Nanotechnology
Nanotechnology **35** (2024) 225702 (9pp)
https://doi.org/10.1088/1361-6528/ad2bce

Preparation of multilayer samples for scanning thermal microscopy examination

James Lees[1], Marco Corbetta[2], Matthias Kleine-Boymann[3], Adi Scheidemann[2], Siew Wai Poon[1] and Sarah M Thompson[1]

[1] The University of York, Heslington, YO10 5DD, United Kingdom
[2] NanoScan AG, Hermetschloostrasse 77, 8048 Zürich, Switzerland
[3] IONTOF, Heisenbergstraße 15, D-48149 Münster, Germany

E-mail: james.lees@york.ac.uk

Received 18 December 2023, revised 8 February 2024
Accepted for publication 21 February 2024
Published 13 March 2024

Abstract

Thin film multilayer materials are very important for a variety of key technologies such as hard drive storage. However, their multilayered nature means it can be difficult to examine them after production and determining properties of individual layers is harder still. Here, methods of preparing multilayer samples for examination using scanning thermal microscopy are compared, showing that both a combination of mechanical and ion beam polishing, and ion beam milling to form a crater produce suitable surfaces for scanning thermal microscopy examination. However, the larger exposed surfaces of the ion beam milled crater are the most promising for distinguishing between the layers and comparison of their thermal transport properties.

Keywords: SThM, HAMR, multilayer materials, magnetic recording materials, thermal transport, scanning thermal microscopy

1. Introduction

An increasing number of technologies make use of stacked thin film layers in their design. These multilayer devices rely on their composite nature for their functionality in a wide range of sectors. However, the individual buried layers are often inaccessible to analysis techniques, and measurements of the material as a whole cannot always provide the required information. There is therefore a demand for techniques which can access the properties of buried layers, in this case thermal analysis of thin layers within a multilayer stack. An example of such a technology is heat-assisted magnetic recording (HAMR) which relies on being able to heat up and then rapidly dispel heat from a small, localised volume [1, 2], making heat transport a critical material design criteria. The thermal transport properties of the magnetic media are particularly critical where anisotropic heat transport properties are desirable to inhibit lateral heat transport between neighbouring bits, but good vertical heat transport out of the media [3]. High thermal conductivity dielectric materials are a key component here.

The understanding of thermal transport on the nanoscale lags behind that of electrical transport and hence there is an even greater need for techniques capable of spatial and depth resolution.

Measurement techniques such as thermoreflectance or bulk examinations do not readily capture heat flow in the buried layers [4]. In this paper, the capability of scanning thermal microscopy (SThM) [5] combined with different ways of cross-sectioning to expose the multilayers is explored as a method for examining the thermal properties of multilayer materials.

SThM is usually performed using a contact mode atomic force microscope (AFM) where the usual passive topography probe is replaced with a probe that has a temperature-sensitive element integrated in it. This allows for simultaneous topography and thermal measurements with a high spatial resolution [6, 7]. Most commonly, as in this work, the SThM tip acts as a resistance thermometer through which an electrical current is passed. The probe temperature is therefore the resultant of both the Joule heating of the tip and the heat flow

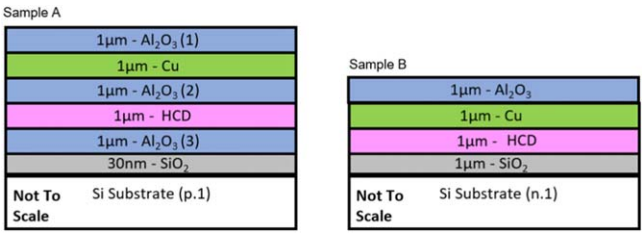

Figure 1. Diagram of multilayer samples A (left) and B (right). HCD is a high thermal conductivity dielectric material.

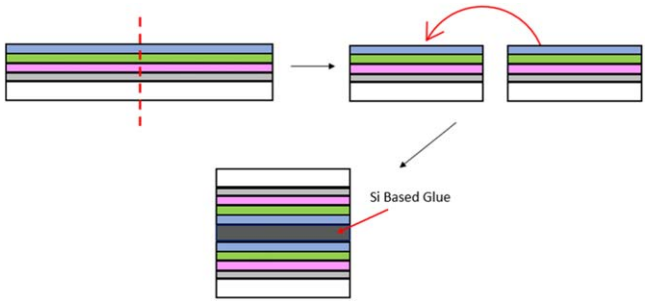

Figure 2. Diagram of process of preparing a multilayer with the 'cut and polish' method by cutting the sample and using a silicon-based glue (grey) to attach one section to the other.

between the sample and the tip. The resulting temperature map therefore contains information about the thermal transport properties of the material as well as the temperature profile of the surface. The tip can be operated in 'active' mode where the tip is Joule heated to a higher temperature than the surface or in 'passive' mode where it is the surface that is hotter and the tip current is acting primarily as a sensing current. In active mode the tip is optimised for sensing the material properties, and in passive mode, the surface temperature.

The heat paths between the tip and sample are important to consider. Heat can be transferred through solid–solid contact but also through a condensed water meniscus and the surrounding gas. Whilst the solid–solid conduction is the most efficient method, the relative scale of the contact area means that for these probes it accounted for only $\sim$10% of heat transfer. Due to the much larger contact area, the water meniscus on the other hand contributed about 88% of the heat transfer with the gas the remaining 2% [8, 9].

The contribution of the contact area of both the probe and the surrounding water meniscus means that anything which affects the contact area, such as tip shape, topographical features and surface roughness, will also affect the thermal measurements. Therefore, a smooth and flat surface is highly desirable for an SThM measurement as it limits the error caused by a change in the contact.

Two methods of sample preparation were tested as candidates for SThM study of multilayers. One used a 'cut and polish' method such as is commonly used for cross-section transmission electron microscopy the other an ion beam milling crater method. Previous work by the group of Professor Oleg Kolosov at the University of Lancaster has resulted in the development of a proprietary ion-milling technique able to produce sub-nm roughness in some materials [10].

2. Methods

2.1. Sample preparation

Two samples were used in this study; samples A and B, as shown in figure 1. The majority of the experiments and simulations were performed on A samples. These consisted of layers of Al_2O_3, Cu, and a high thermal conductivity dielectric material (HCD). These materials and their arrangement were chosen to provide a contrast between materials with very different thermal conductivities to compare to the HCD. Note that two different Si substrates were used where samples A were grown on a p-type Si (B-doped, 0.005–300 Ω.cm resistivity) and samples B were grown on a n-type Si (P-doped, 0–100 Ω.cm resistivity).

The simplest way to expose the various multilayers is to cut the sample in such a way that the cross section is visible. This is a standard method of transmission electron microscope sample preparation [11]. The samples were extracted from the wafer using a diamond dicing saw (DISCO DAD-320) and then stuck together using a Si based glue on the top surface as shown in figure 2. The assembled sample was then diced again with the diamond saw ready for polishing. This was first done mechanically using a series of lubricated diamond polishing mats of decreasing roughness from 30 to 0.5 μm with each sequentially smoothing the surface. A rotary plate was used to speed up the initial coarse polishing steps. A final polish using a 0.3 μm Si polishing grit was also performed.

Initial SThM scans demonstrated that the mechanical polishing did not result in a smooth enough surface, so a final step of ion beam polishing was added. For this, a homogeneous exposure of Ar^+_{1600} at 20 keV and 14.05 nA for 30 s was used.

The second method relied entirely on ion beam milling to mill into the surface of the wafer to expose the multilayers by creating a shallow gradient crater.

All the ion beam milling was performed at IONTOF in a time-of-flight secondary ion mass spectrometry (ToF-SIMS) instrument equipped with an argon gas cluster ion source [12]. Ion beams are typically directed onto a sample at an angle in order to smooth non-regular surfaces. Within a multilayer however, the ability to produce a highly flat surface is hindered by the fact that the different materials mill at variable rates under the same exposure. This preferential etching means that longer exposure periods can result in a less even surface than shorter ones. The exposure can also result in ridge patterns caused by the beam.

By exposing a material to an ion beam for an extended period, it is possible to use the milling to actively drill down into a surface. If carefully controlled in a multilayer this can be used to expose the buried layers. The depth milled into the surface can be controlled by altering the dose (controlled by the dwell time) of the ion beam as it is scanned along a

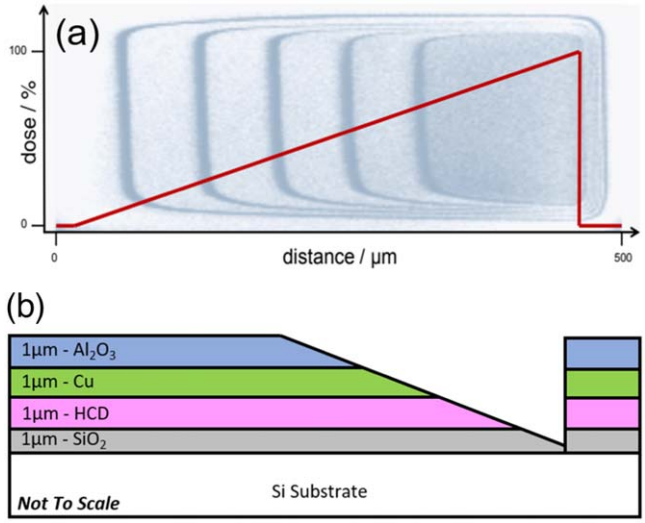

Figure 3. (a) Graph and diagram describing increasing dosage use to cause ion mill exposed multilayer. (b) Cross sectional diagram of ion mill crater multilayer sample B showing how layers are exposed as a surface with a gradient.

surface. By gradually increasing the dose along the *X* axis a wedge-like crater is created which exposes the layers. As long as the gradient is sufficiently shallow (such that the measured height change does not exceed the AFM's depth range of 10 microns) the exposed layers are then accessible to examine using an SThM. The resulting cross-section is shown in figure 3.

The milling parameters were varied in order to optimise the surface of the cross-section to produce one which was deep enough to expose all of the different layers and keep a smooth surface. The dwell time of the beam was varied from 10 to 300 ms pixel^{-1}, the sputter current between 14.05 and 14.658 nA, and different sputter species Ar^{+}_{1600} and Ar^{+}_{1370} were tested.

2.2. Scanning thermal microscopy

All SThM measurements in this paper were performed in contact mode using a NanoScan VLS-80 AFM with the conventional AFM probe replaced with a temperature-sensitive Pd coated thermal probe KNT-SThM-2an from Kelvin Nanotechnology [13]. This probe has a 10 μm tip height, $<$100 nm tip radius, a typical spring constant of 0.40 N m^{-1}, and a thermal sensitivity of 1 Ω K^{-1}. All data analysis was performed using Gwyddion [14].

The small changes in electrical resistance due to temperature changes of the tip were detected using an electronic bridge circuit designed by the group of Professor Oleg Kolosov from Lancaster University [15]. At the same time, the optical feedback of the AFM is maintained for two reasons, firstly in order to capture the topography information simultaneously and also to maintain a constant contact between the tip and surface. This set-up results in a thermal spatial resolution of 100 nm and a thermal resolution of $<$10 mK.

Note that measurements of absolute temperature are not accessible by this method, only variations in temperature which are correlated to the measured change in a bridge voltage. The recorded tip temperature will be changed by any difference in the tip/sample heat flow. This has three main factors: the temperature difference between the tip and the surface, the thermal properties of the surface and the thermal contact resistance. The spatial variations in tip temperature are therefore directly related to spatial variations in thermal transport properties close to the surface. However, due to the contact area being a significant factor, topographical features can also cause a detectable change in the thermal signal as the changing tip/sample contact will result in varying solid–solid contact area.

2.3. Finite element simulations

COMSOL [16] was used to simulate the SThM response to the different methods of examining multilayered materials i.e. from the top surface of the complete stack, the cut and polish method and the ion-milled crater. The SThM response could then be simulated for different layer thicknesses, including the measured values determined by SThM scanning and the idealised sample thicknesses (where all layers are 1 μm thick).

The modelled COMSOL tip consists of a 100 nm radius semicircle constructed of an Si_3N_4 core of 40 nm radius, an inner layer of Pd with an 80 nm radius and a final outer shell of Si_3N_4 as can be seen in later diagrams. A small current is supplied to the Pd layer causing some joule heating. The tip temperature is measured as the area average temperature of the Pd layer of the tip, which is affected when the tip is in contact with other materials. The COMSOL model required the use of the Heat Transfer and AC/DC modules.

For boundary conditions the bottom of the Si substrate was set to a constant room temperature of 20 °C. All of the surface vertices were set using the COMSOL inbuilt functions to convect to air as if in atmospheric conditions of 1 atm and 20 °C.

The contact area between the tip and the surface is calculated within the simulation as a disk at the geometric intersection of the two beyond which the sample remains, and the tip is deleted. Thus, the contact resistance is largely calculated as a factor or the size of this intersection which is determined by contact angle.

3. Results and discussion

3.1. Sample topography and roughness

A secondary ion mass spectrometry (SIMS) examination of the ion milled craters was also performed as shown in figure 3 revealing the different elements exposed in the different layers. This was done at various stages to see how far into the multilayer the ion beam cut had reached as shown schematically and as an optical image in figure 4.

When considering the surface suitability for SThM examination there are a number of important factors. The size

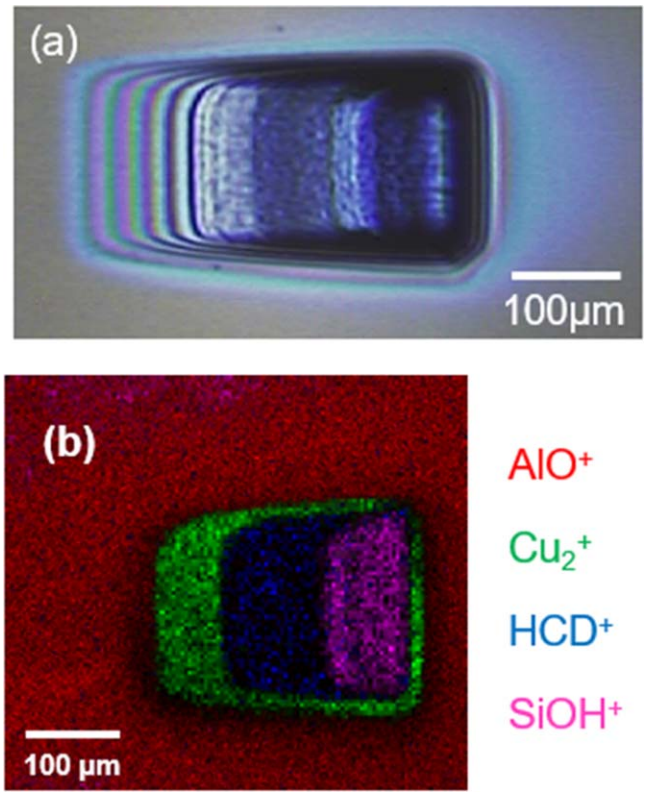

Figure 4. (a) Optical image of ion milled wedge crater with steep gradient on right side and shallow gradient on left. (b) SIMS image of ion milled crater with key for different recorded ions from the surface.

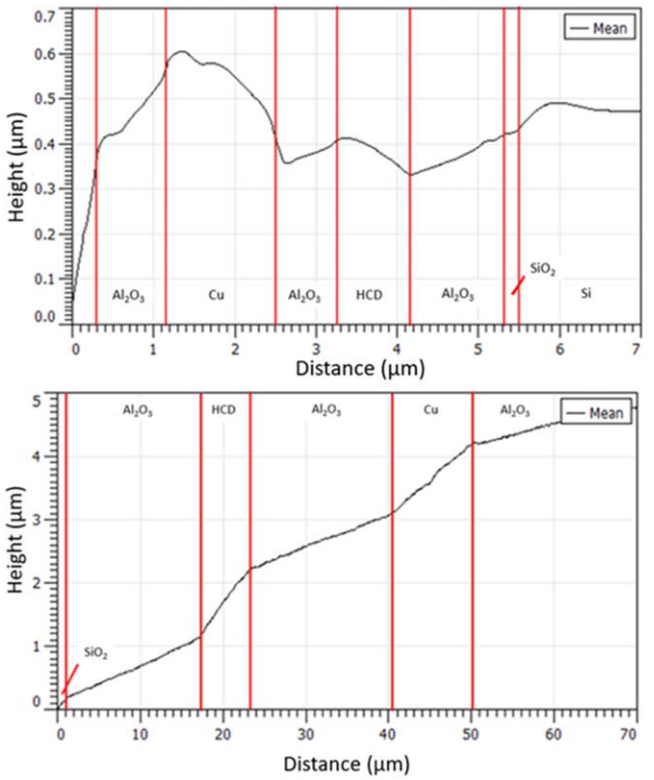

Figure 5. Line averaged topography graphs of sample A for 'cut and polish' (top) and ion milled crater (bottom). Note that the two graphs are laterally inverted.

of the available scanning area is important (a larger area enabling more averaging), but so too is the roughness of the surface and also the macro surface features (i.e. those significantly larger than the tip).

A simple comparison between macro roughness of the two different methods can be made by examining the recorded topographies. Figure 5 shows the line-averaged topography scans for a cut and polished and ion milled crater samples—note the approximately 10× scale difference in the *y*-axis, which accentuates the macro-scale variations for the cut and polish sample.

The cut and polished sample is nominally flat (i.e. no gradient) and hence the macro scale variations which coincide with the different materials are likely due to effects such as different degrees of oxidation or polishing variation across the surface. The ion milled crater shows the shallow gradient of the crater and the different gradients resulting from the preferential etching of the different layers. The small-scale roughness of each of the material surfaces is further explored in the roughness analysis.

The RMS Roughness was measured across all the recorded image scans of the samples and averaged to provide an overall average layer roughness for their respective methods. This information is shown in tables 1 and 2 where the error is calculated from the averaging across the sample.

Throughout the ion beam milled crater samples, across all materials, a series of ridges were seen as shown in figure 6.

Table 1. Table of RMS surface roughness of cut and polish layers.

Layer	RMS roughness (nm)	Error (nm)
Al_2O_3 (1)	42	±7
Cu	67	±2
Al_2O_3 (2)	35	±7
HCD	33	±7
Al_2O_3 (3)	32	±8
SiO_2	19	±5

Table 2. Table of RMS surface roughness of ion beam crater layers.

Layer	RMS roughness (nm)	Error (nm)
Al_2O_3 (1)	81	±13
Cu	156	±18
Al_2O_3 (2)	87	±12
HCD	99	±22
Al_2O_3 (3)	82	±11
SiO_2	31	±11

These ridges had a consistent width of around 300 nm, and a variable height depending on the material. These ridges are a significant contributory factor to the surface roughness measurement.

The comparison clearly shows a much smoother surface for the cut and polish which does not suffer from the ion milling induced ridges on the milled crater. It should be noted however that the Cu surface was significantly affected by

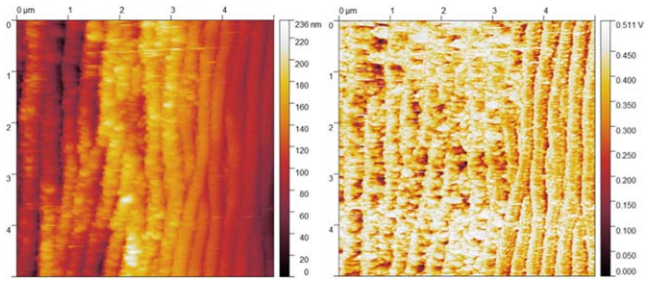

Figure 6. Example SThM images of ion-beam produced ridge features at the Cu-Al_2O_3 (left and right respectively) interface, topography (left) in nm and thermal (right) in V which directly correlates to the heat transfer to the surface. Taken at 5 × 5 μm^2 512 × 512p, 1.4 s/line 30 nm setpoint.

oxidation from exposure to air between ion beam preparation and introduction to the AFM. Attempts performed several months later to examine the surface were by then impossible due to the oxidised surface becoming too rough.

It is clear both of the preparation methods are able to expose the multilayers and result in surfaces which are examinable using SThM however there are a number of differences between the two. The 'cut and polish' samples have on average smoother surfaces (38 nm RMS) across the different materials compared to the ion mill (86 nm RMS), primarily due to the presence of the ridges which are caused by the ion milling. However, the surface of the 'cut and polish' has resulted in larger scale topographical variations which affect the tip-surface contact as seen in figure 5.

3.2. Thermal imaging

The major advantage of the ion milled crater is that the wedge shape exposes a significantly larger surface area for each material which can be examined by the SThM and then averaged to reduce the statistical error. This is because the 'cut and polish' method is limited by the thickness of the layer whereas the crater exposes along a gradient creating a greater examinable material width for the same layer thickness. Not only does this allow for better averaging of results but it also reduces the influence of edge effects.

Figure 7 shows examples of line averaged tip voltages (i.e. the average for each column position of values of the 2D cross section) for samples prepared by the two methods. The different surface roughness and thermal properties of the exposed layers result in different resultant tip temperatures and delineation between the layers. In examining the thermal line average graphs, whilst the statistical error for the cut and polish is smaller the larger changes from the surface dominate the measurement.

The ion milled graph in figure 7 shows a clear difference between the measured voltage for the layers which is caused by their different thermal conductivities. Cu and the HCD show a lower voltage than the Al_2O_3 which comes from their higher κ cooling the tip more effectively.

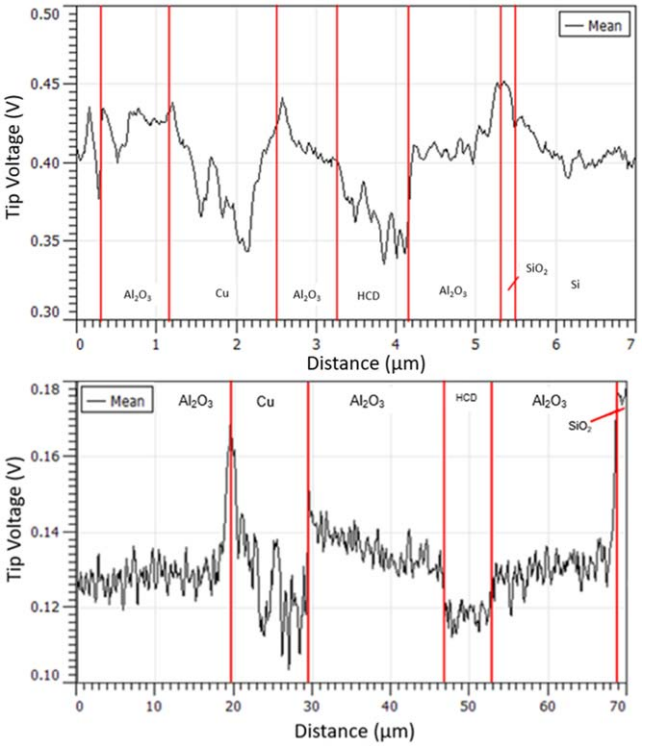

Figure 7. Thermal line averaged scans for the 'cut and polish' (Top) and ion milled crater (Bottom) samples.

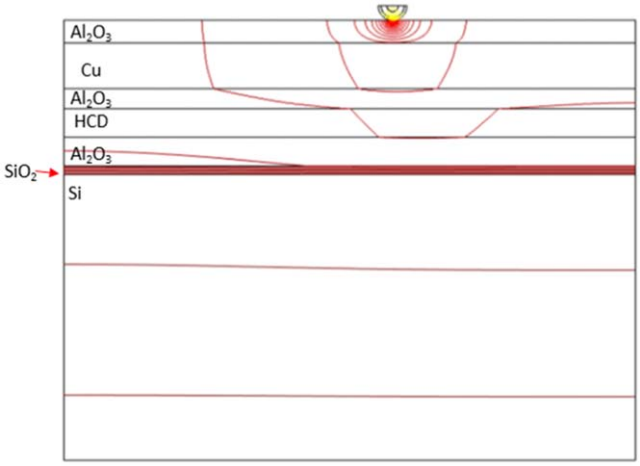

Figure 8. Image of COMSOL model of heated tip over multilayer stack showing thermal contours travelling through different material layers.

3.3. COMSOL simulations

Figure 8 shows the simulated response of the heat map resulting from a heated tip being scanned across the top surface of the multilayer stack (i.e. without preparation) with the shape of the contours affected by the different thermal transport properties of the different layers.

Figure 9 shows the temperature of the tip as a function of its position on the surface of the multilayer stack (resulting from both the Joule heating and the heat loss from the tip on contact with the surface) which shows a combination of edge effects and mesh size limitations. Simulations are compared

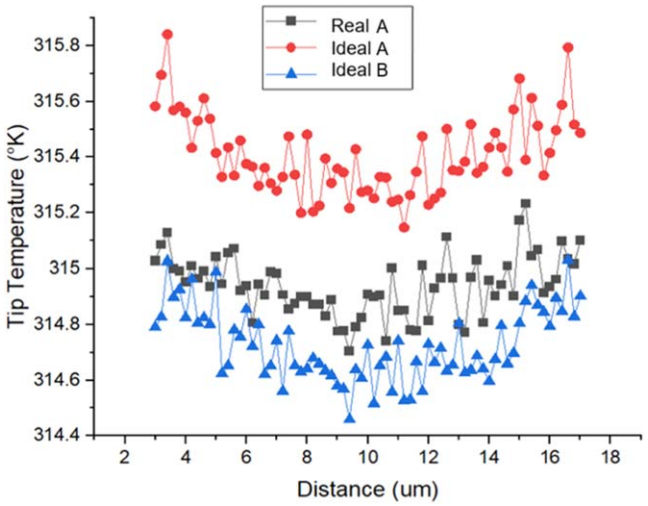

Figure 9. Tip temperature for simulated multilayer stacks of idealised A and B samples (i.e. 1 μm layer thickness) and a model using layer thickness measured using SThM scanning detailed in table 1 with extreme edge effects removed.

Table 3. Experimentally measured thickness using AFM imaging of multilayers and thermal conductivity values for the bulk material taken from COMSOL library.

Layer	Thickness (μm)	Error (μm)	κ (w/mK)
Al_2O_3 (1)	0.8	±0.2	35
Cu	1.6	±0.3	400
Al_2O_3 (2)	0.7	±0.2	35
HCD	1	±0.1	321
Al_2O_3 (3)	1	±0.1	35
SiO_2	0.3	±0.1	1.4
Si	—	—	130

between the two idealised stacks A and B and a stack using the measured thicknesses of the actual sample. These thicknesses as well as the COMSOL library values for thermal conductivity are detailed in table 3. The three simulations all show the same curved shape with the temperature higher at the edges of the sample where the heat paths are shortened.

The different layer thicknesses and proximity to the surface of the three samples result in differences in the heat flow from the tip and hence different overall tip temperatures.

Determining thermal properties by examining just the surface would be very difficult as it would require comparing small changes in absolute temperature between the samples which is prone to large systematic errors when using a bridge detection method. This could be mitigated by preparing specially designed samples where a single factor (such as the layer thickness, or composition of an individual material) is changed over the length of a scan so that the properties can be deduced from the changes detected. This highlights the need for an ability to access the buried layers.

All further simulations were performed using the A sample.

The 'cut and polish' method was simulated by moving the tip and its motion onto the side of the COMSOL model as

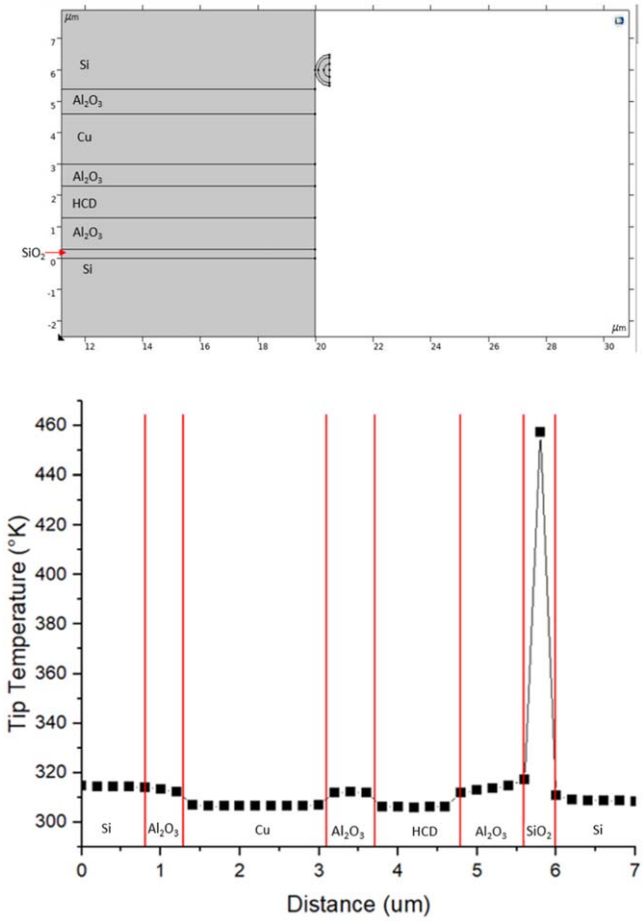

Figure 10. Image of COMSOL model of tip passing over the 'cut and polish' surface with an additional Si layer to prevent significant edge effects (top) and simulated tip temperature (bottom).

shown in figure 10 with an additional Si layer to simulate the Si based glue used to attach the two parts of the sample together and reduce edge effects.

A number of very clear features are visible in figure 10. The different layers are clearly distinguished by the different tip temperatures. These differences are consistent with the different thermal conductivity values for the different layers as listed in table 3 i.e. the layers with higher κ values result in a lower tip temperature due to their ability to transport heat away from the tip more efficiently. Heat also diffuses laterally away from the tip, resulting in temperature changes towards the edges of the layers.

This method shows potential for the thickness of each layer to be determined as well as the relative thermal conductivities of the layers.

In order to simulate the ion milled crater sample, the topography of the milled sample had to be recreated. This required matching the topography of a measured sample to each layer of the sample due to the preferential etching which resulted in a nonlinear gradient into the sample. This then required the path of the tip to be mapped onto the sample surface as shown in figure 11.

The resulting graph of tip temperature in figure 11 looks very similar to that obtained from the 'cut and polish' method shown in figure 10. Both of them show similar temperature

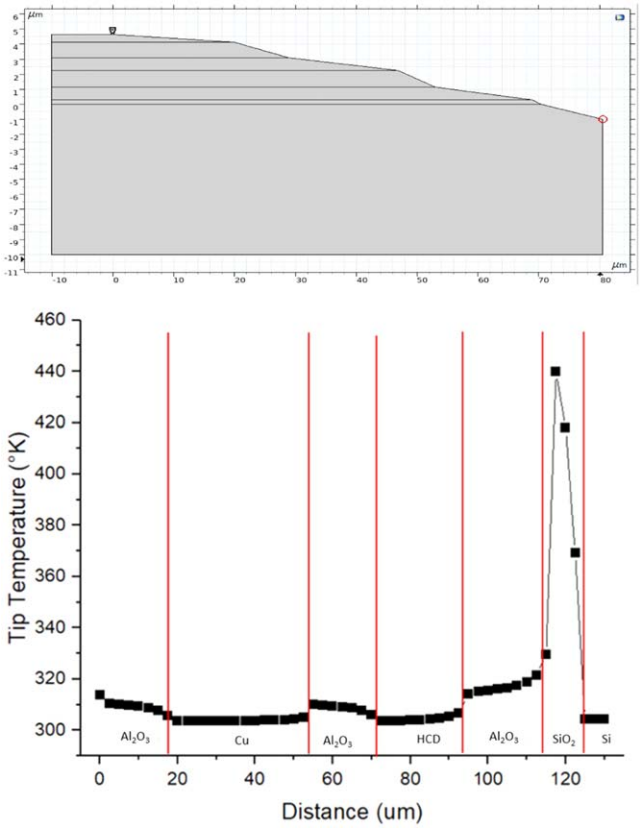

Figure 11. Image of sloping gradient COMSOL model of ion milled crater with realistic multilayer gradients applied. Note 1:3 scaling in X (top) and simulated tip temperature (bottom).

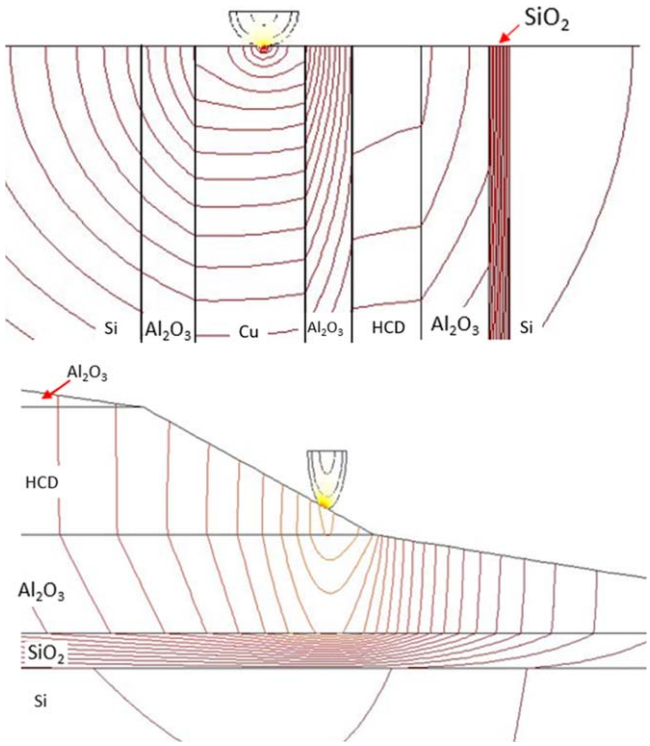

Figure 12. Representative diagrams showing tip/sample heat paths for the 'cut and polish' sample (top) and for the ion milled crater sample (bottom). Note that the ion milled crater has been compressed along the *X* axis at a 1:3 ratio to allow for easier examination.

differences between the layers and the same distinct features such as the SiO_2 peak.

There are two main differences between the models for the different preparation methods. The first is that they present different heat paths from the tip into and through the sample. As shown in figure 12 the 'cut and polish' sample has the tip in contact above a single material which is flanked by others. This means that the tip temperature measurements are mostly of a single material but there are larger edge effects. These are seen as thermal gradients as the influence of the adjacent material becomes stronger. The ion milled crater on the other hand has a more immediately complex heat path as there is a greater impact in the local area from other materials which varies along the length of the scan.

The second difference is that the milled surface has a much greater exposed layer thickness. This allows for more data points to be taken across the surface at the same sampling rate and fewer of these data points will be significantly impacted by edge effects. This results in better averaging and reduced noise.

4. Discussion

The measured thermal line average of the ion milled crater can be compared to the COMSOL model version of the same as seen in figure 13.

There are some clear similarities between the experimental data and the model, with the magnitude of the thermal signals for the different layers showing similar sized changes and hence qualitative correlation with the thermal transport properties of the different layers. No calibration curve was taken for this measurement and as such a direct comparison between the relative tip temperature changes of the model and measurement cannot be made.

One of the largest differences is the much higher peak seen in the model data for the SiO_2. This is likely due to the edge effects caused by the interfaces in the experimental data which are not fully accounted for in the COMSOL model. This large peak in the modelled SiO_2 also affects the adjacent Al_2O_3 layer making the detected temperature higher than is seen on the experimental data.

Further differences can be seen on the first (leftmost) Al_2O_3 layer which were likely caused by the shortened heat path to the edge like those seen in figure 9.

The model is limited by a number of factors, not least that it assumes all the materials and interfaces to be perfect which results in more efficient heat transport than reality. The modelling of the tip also does not include a cantilever which can have significant effects on the tip cooling which are not modelled here. Additionally, the water meniscus that forms around the tip-surface contact [6] has been ignored in the simulation. Only solid–solid contact with a simple change in the thermal contact radius is simulated here, the inclusion of the meniscus would likely affect this further. When making

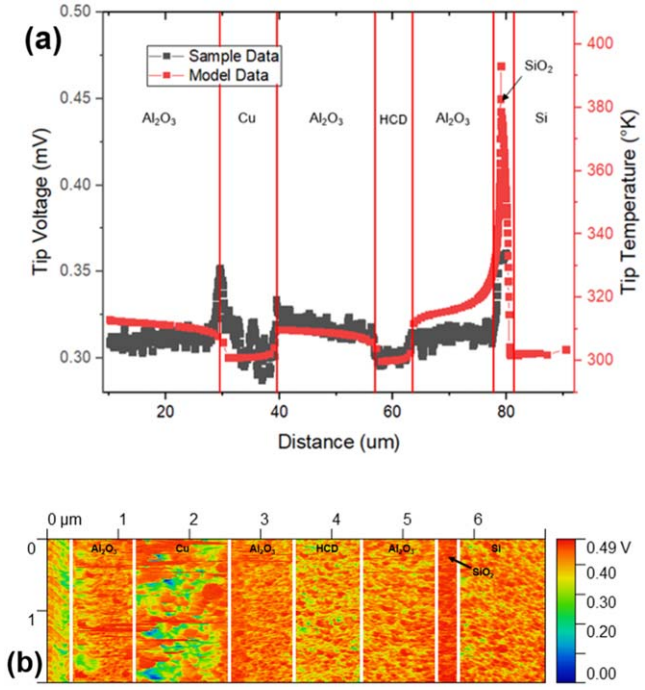

Figure 13. (a) Graph comparing thermal signal from ion milled crater sample and tip temperature from the crater gradient COMSOL model. (b) representative SThM thermal image.

comparisons between aeras of the sample with different thermal transport, these factors are mitigated by the areas having similar and very smooth surface topography.

Because of the more clearly delineated layers and the ability to expose surface areas of materials that are not strictly limited by the layer thickness, the ion milled crater method is the preferable sample preparation technique despite the rougher surface.

It is possible to create an even shallower gradient by slowing down the rate at which the dosage is increased whilst milling the surface and increasing the physical length that is milled. This could then be used to examine very thin layers which would not be thick enough for meaningful analysis using the 'cut and polish' method, additionally such a method would increase the measurable area away from an interface.

5. Conclusion

Both preparation methods, 'cut and polish' and 'ion beam milling' produced surfaces suitable for examination with SThM.

For the 'cut and polish' method, it was found that both a manual and ion beam polish were required and that a 30 s ion beam polish resulted in the smoothest surface as a trade-off between the polish and preferential etching. The ion beam milling method resulted in a rougher surface than the 'cut and polish' method due to the ridges produced.

However, the significantly larger surface area over which the examinations can be performed resulted in the ion milled crater being the preferable sample preparation method as it can expose thinner layers and resulted in a greater revealed surface area which allows for better averaging of measurement noise. COMSOL simulations were also performed which mimicked the geometry of the preparation methods and were found to have good qualitative agreement.

It has been shown that by using highly controlled ion beam milling to create a shallow crater, it is possible to use SThM thermal data to distinguish between layers in multi-layered samples and to make qualitative statements about the relative thermal conductivity of the materials. The data quality would be improved by reducing the surface roughness, and particularly the ion-milling ridge effect. Further improvements to the technique could be made by including a thermally well characterised material included in the scans for comparison.

Acknowledgments

With thanks to Seagate for the provision of the samples. We acknowledge the support of EPSRC Grant EP/R513386/1.

Data availability statement

The data that support the findings of this study are openly available at the following URL/DOI: https://doi.org/10.15124/c3130def-4f6e-4055-89f7-f3eeb152a7b7.

ORCID iDs

James Lees https://orcid.org/0000-0001-8566-3935
Matthias Kleine-Boymann https://orcid.org/0000-0002-1632-5120

References

[1] Kryder M H *et al* 2008 Heat assisted magnetic recording *Proc. IEEE* **96** 1810–35
[2] Bain J A, Malen J A, Jeong M and Ganapathy T 2018 Nanoscale thermal transport aspects of heat-assisted magnetic recording devices and materials *MRS Bull.* **43** 112–8
[3] Weller D *et al* 2014 A HAMR media technology roadmap to an areal density of 4 Tb/in^2 *IEEE Trans. Magn.* **50** 1–8
[4] Cahill D G, Goodson K and Majumdar A 2002 Thermometry and thermal transport in micro/nanoscale solid-state devices and structures *J. Heat Transfer* **124** 223–41
[5] Menges F, Riel H, Stemmer A and Gotsmann B 2016 Nanoscale thermometry by scanning thermal microscopy *Rev. Sci. Instrum.* **87** 074902
[6] Gomès S, Assy A and Chapuis P O 2015 Scanning thermal microscopy: a review *Phys. Status Solidi*a **212** 477–94
[7] Nonnenmacher M and Wickramasinghe H K 1992 Scanning probe microscopy of thermal conductivity and subsurface properties *Appl. Phys. Lett.* **61** 168–70
[8] Majumdar A 1999 Scanning thermal microscopy *Annu. Rev. Mater. Sci.* **29** 505–85
[9] James L 2022 *Spatially Resolved Nanothermal Transport of Multilayer and Phononic Structures using Scanning*

Thermal Microscopy University of York Available from: https://etheses.whiterose.ac.uk/30836/1/James%20Lees%20-%20PhD%20Thesis%20FS.pdf

[10] Kolosov O V and Grishin I 2016 *Method for Ion Beam Polishing and Polished Sample* EP 2 537 017 B1 Available from: https://patentimages.storage.googleapis.com/4d/b6/d1/4b9519c706824f/EP2537017B1.pdf

[11] Weaver L 1997 Cross-section TEM sample preparation of multilayer and poorly adhering films *Microsc. Res. Tech.* **36** 368–71

[12] IONTOF—TOF-SIMS (time of flight secondary ion mass spectrometry)—LEIS (low energy ion scattering) Available from: https://iontof.com/tof-sims-5-product-version-100mm-200mm-300mm.html

[13] AFM Probes Kelvin nanotechnology Available from: https://kntnano.com/probes/

[14] Nečas D and Klapetek P 2012 Gwyddion: an open-source software for SPM data analysis *Cent. Eur. J. Phys.* **10** 181–8

[15] Timofeeva M, Bolshakov A, Tovee P D, Zeze D A, Dubrovskii V G and Kolosov O V 2015 Scanning thermal microscopy with heat conductive nanowire probes (https://doi.org/10.1016/j.ultramic.2015.12.006)

[16] COMSOL—software for multiphysics simulation Available from: https://comsol.com/